

ECE 698: Final Report

Constructing a Raman Spectroscopy System

**Author:**

Jake Nguyen  
Student in Computer Engineering

**Faculty Adviser:**

Dr. Hani Elsayed-Ali

**NASA Adviser:**

Dr. M Nurul Abedin

Old Dominion University  
Department of Electrical and Computer Engineering  
December 8<sup>th</sup>, 2023

**Honor Code:**

ODU Honor Code must be adhered to. This means that homework assignments and design projects are to be the work of an individual student group only. Evidence such as identical results and/or wording of sections of a report, if strong enough, will be reported to the University Hearing Officer in charge of administrating the ODU Honor Code. If the violation is deemed sufficient, a permanent record of this infraction will be placed on the student's official university transcript for the first offense! Subsequent offenses could result in dismissal from the university.

## **Acknowledgment**

I would like to take this opportunity to sincerely say many thanks to NASA LaRC and especially Dr. M Nurul Abedin for welcoming me and gave me a chance that I never thought I would be able to have. I am deeply appreciated for everything I have learned and from my mistakes. This was truly an experience that will be hard to forget.

### **Abstract:**

The project aims to understand how Raman spectroscopy works by constructing a system based on existing concepts of the technique and utilizing NASA's available tools and software to analyze the collected data. Once the data is successfully interpreted and proven, other improvements to the assembled system will then be explored. Part of the paper goes through several phases of construction of the system and improvements made. Nevertheless, the data obtained and the results were unsatisfactory as they need to be further analyzed for accuracy. The ultimate ambition was to be able to assist NASA with its objective of implementing a remote and compact Raman spectroscopy system on a rover for future planetary surface characterization such as Mars and lunar surfaces via a Raman spectroscopy system that the agency's Senior Engineer, Dr. M. Nurul Abedin, has been working on since the early 2000s [2,3,4].

## Table of Contents:

1. Introduction .....	5
2. Construction.....	5
i.    Mirrors - set at around 45° to guide laser beam.....	6
ii.   Neutral Density filter – laser beam intensity reduction.....	6
iii.  ST-133 Controller.....	6
iv.   Semrock 785 nm RazorEdge Dichroic™ laser beamsplitter .....	6
v.    785 nm StopLine® single-notch filter.....	6
vi.   Crystalaser 785nm Continuous Wave (CW) Laser .....	6
vii.  HeNe 632.8 nm CW laser .....	6
viii. Optical lens .....	6
ix.   Kaiser Optical System Spectrometer .....	6
x.    Intensified Charge-coupled Device Camera System (ICCD) .....	6
xi.   Sulfur Crystal sample .....	6
xii.  Naphthalene sample.....	7
xiii. Calcite sample .....	7
Phase 1 .....	6
Phase 2 .....	9
Phase 3 .....	10
3. Overall Results and Analysis .....	13
4. Summary / Conclusion .....	14
5. Reference .....	15

## List of Figures

Figure 1: Block diagram of Phase 1 setup .....	7
Figure 2: Top view of the spectrometer setup in Phase 1 .....	8
Figure 3: 632.8 nm HeNe laser peak obtained in Phase 1 .....	8
Figure 4: Block diagram for Phase 2 setup .....	10
Figure 5: Top view of the block diagram of the system in Phase 3 .....	11
Figure 6: Neon source upper and lower spectrum .....	11
Figure 7: Peaks in lower and upper regions of the neon source .....	12
Figure 8: Peaks obtained from sulfur sample with a 785 nm CW laser .....	12
Figure 9: Pixel to wavelength conversion values .....	13
Figure 10: Inconclusive Raman peaks of sulfur .....	14

## Equations

Equation 1: EFL .....	10
Equation 2: Ratio of nm/pixel formula .....	12
Equation 3: Pixel to wavelength conversion formula .....	13
Equation 4: Raman shift formula .....	13

## 1. Introduction

Raman scattering is a non-linear optical phenomenon and Raman spectroscopy is a non-destructive technique used to study molecules' vibrational, rotational, and other low-frequency modes. When molecules scatter light, the scattered light can output different frequencies or energy levels due to interactions with molecular vibrations. The shift in frequencies coming off from the illuminated molecule is unique to the molecule and type of bonds and the frequencies can help determine which molecules are present in the sample [1, 6]. There are typically three Raman events that may occur in what is known as the relative shift in energy of the incident light photon energy. First of all, Raman scattering is non-linear because it involves a change in the energy of the scattered photons, which is not proportional to the energy of the incident photons. When the incident photons interact with the molecules in the sample, most of the scattered photons retain their original energy or wavelength [1, 6, 9]. This is known as Rayleigh scattering (inelastic) or linear. In Raman scattering (non-linear), a small fraction of the incident photon interacts with molecules in specific ways, resulting in energy exchange between the photons and the molecules. Specifically, when a photon interacts with a molecule, it can either gain (anti-stokes) or lose energy (stokes) depending on the molecular vibrations and rotations [1, 6, 9]. The scattered photons have energies that differ from the incident photons, leading to a non-linear relationship between the incident and scattered photon energies. This non-linear energy exchange or shift in energy is known as the Raman shift, which allows Raman spectroscopy to provide information about the vibrational and rotational modes of molecules, making it ideal for identifying, characterizing, and quantifying many chemical components and molecular structures. In Stokes Raman scattering, the scattered photons have lower energy compared to the incident photons. This happens during the interaction when the photon gives up its energy to a molecule as it scatters, resulting in the excitation of a higher vibrational energy level within the molecule. Stokes scattering is also the more common of the two types. The second type is Anti-Stokes Raman scattering, where the scattered photons have higher energy compared to the incident photons. Anti-Stokes scattering occurs when a photon gains energy from a molecule as it scatters, resulting from the de-excitation of a higher vibrational energy level in the molecule [1, 6, 9]. This type of scattering is less common and generally weaker than Stokes scattering because it requires the molecules to already be in a higher vibrational energy state, which is typically from thermal excitation.

## 2. Construction

NASA's original design consisted of a pulsed 532 nm wavelength laser, which is lined up alongside the telescope system with a 4-inch aperture [2]. The laser beam's direction is guided through two 45° prisms, then strikes the sample. The photon scatter will then be transmitted through the telescope through a 20x microscope objective lens before entering the spectrograph and onto the ICCD camera. The spectrograph will typically have a series of optical lenses, a notch filter, a slit, and a Volume Phase Holographic (VPH) Diffraction Grating [2]. The VPH Diffraction Grating disperses incoming light into its component wavelengths and colors. The

Intensified Charge-Coupled Device (ICCD) camera is a specialized type of digital imaging device used for capturing and recording high-speed and low-light-level events.

**Equipment/Components:**

- I. Mirrors - set at around 45° to guide laser beam
- II. Neutral Density filter – laser beam intensity reduction
- III. ST-133 Controller
- IV. Semrock 785 nm RazorEdge Dichroic™ laser beam splitter
  - i. Transmission Band =  $T_{avg} > 93\%$  795.2 – 1213.8 nm
  - ii. Reflection Band =  $R_{abs} > 94\%$  785 nm
  - iii. Angle of Incidence = 45 degrees
  - b. Beam splitter reflects laser line at incident angle of 45° while transmits the longer Raman-shifted wavelengths. It is optimized for reflecting laser beams up to 2.5 mm in diameter.
- V. 785 nm StopLine® single-notch filter
  - a. StopLine single-notch filter provides high transmission and a laser-line blocking with  $OD > 6$  for maximum laser rejection. The rejected light is reflected for alignment and stray light control.
  - b. Optical density (OD) – measures the absorption or transmission of light through a highly blocking optical filter. The following equation is the relationship between the transmittance (T) and optical density:
  - c.  $OD = \log_{10} (T)$  where  $T = I/I_0$  ( $I_0$  – incident light intensity;  $I$  – transmitted light intensity)
- VI. Crystalaser 785nm Continuous Wave (CW) Laser
- VII. HeNe 632.8 nm CW laser
- VIII. Optical lens
  - i. 150 mm biconvex
  - ii. 50 mm biconvex
  - iii. Reichert Plan Achromat 20x/0.50 objective lens
  - b. 10x objective lens
- IX. Kaiser Optical System Spectrometer
  - a. Factory-optimized for Raman signal detection
  - b. Includes 4 Nikon camera lens (one 50mm; one Pentax TV Lens 50mm; one AF Nikkor lens, one lens for collection at the exit hole of spectrometer)
  - c. 532 nm notch filter
  - d. 50  $\mu$ m slit
  - e. Raman Diffraction Grating HSG – 632.8 - LF
- X. Princeton Instruments, Inc. Intensified Charge-coupled Device Camera System (ICCD)
- XI. Sulfur Crystal sample
- XII. Naphthalene sample
- XIII. Calcite sample

## Phase 1:

For the initial stage, 632.8 nm HeNe CW laser was used with the construction of the optics system. The schematic in Figure 1 shows a side view of the block diagram of the spectroscopy system's initial setup.

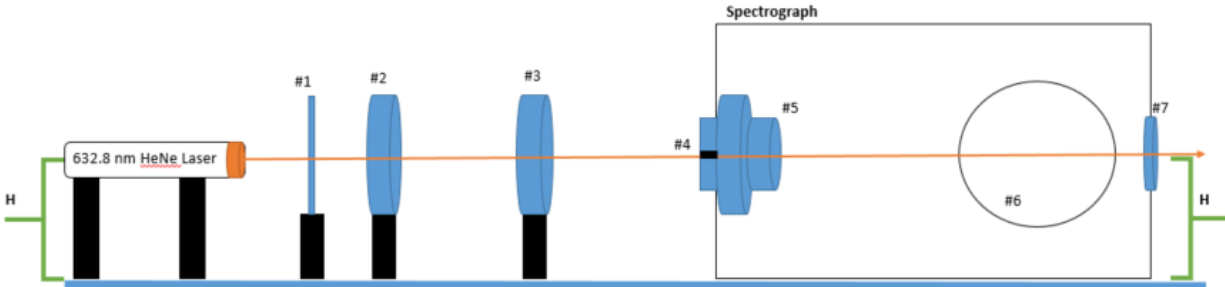


Figure 1: Block diagram of the first setup, sideview. Neutral Density filter (#1, OD of  $\sim 2.0$ ), a 150 mm lens (#2), a 50 mm lens (#3), a 100  $\mu\text{m}$  slit (#4), a 50 mm c-mount biconvex, an exit hole (#7), the central exit hole (#6) that will go through another biconvex lens and to the ICCD camera

The initial biconvex lens, measuring 150 mm in diameter, was positioned approximately 15 cm away from the 100  $\mu\text{m}$  entrance slit for the spectrograph. Following this, there was a second 50 mm lens situated around 5 cm from the slit. After passing through the slit, the beam was directed through another 50 mm biconvex lens within the spectrograph. The objective was to ensure that the beam, upon exiting through exit hole #7, remained at the same height (H) as it was when it left the laser. Exit hole #6 served as the primary exit point, continuing through an additional biconvex lens before reaching the ICCD camera. Figure 2 provides a top view illustration of the spectrometer setup.

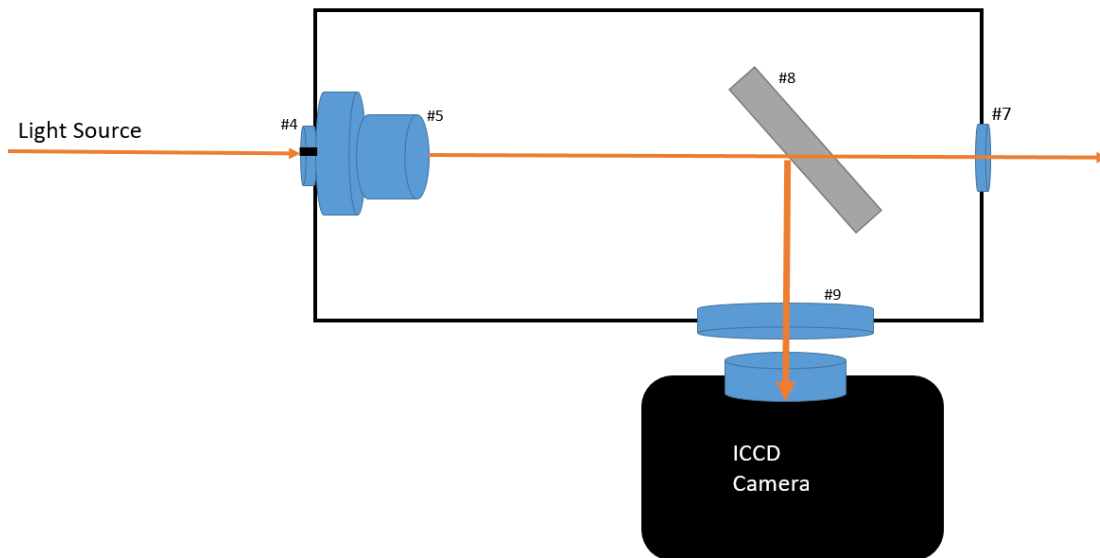


Figure 2: Top view of the spectrometer setup: a 100  $\mu\text{m}$  slit (#4), a 50 mm c—mount lens (#5), a VPH Diffraction Grating (#8), and another biconvex lens (#9).

The goal to observe a signal on a computer screen and began by aligning a HeNe laser with a slit, passing through lenses and a neutral density filter. There were challenges in selecting appropriate equipment to hold the laser, lenses, and filter due to limited resources. This led to multiple trial-and-error attempts to establish an ideal system configuration. Adjustments were frequent because small changes in one component could impact the entire system. External factors like bumps or height adjustments could also alter the laser's path. Finding suitable tools for precise height measurements added to the adjustments. Despite challenges, the difficulties allowed more familiarities with available resources. The current setup secures the HeNe laser with height-adjustable rod holders on a working platform, with lens adjustments facilitated by a rod holder system attached to the spectrograph. Figure 3 displayed a peak that appeared when the HeNe laser was turned on.

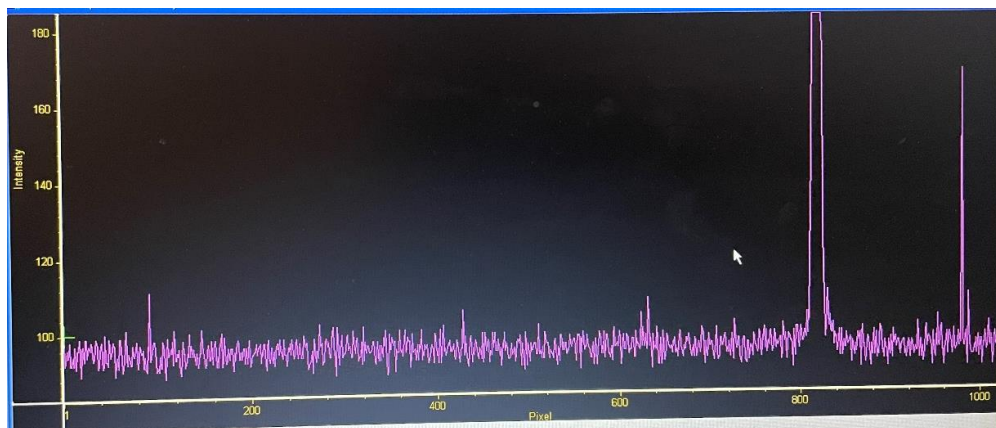


Figure 3: 632.8 nm HeNe laser peak.

An attempt was made to capture the Neon source spectrum by placing it in front of the system alongside the 632.8 nm HeNe laser. To collimate the beam, a 100 mm plano-cylindrical lens was added approximately 8.5 cm behind the 150 mm lens. Despite continuous adjustments to the optical setup and diffraction grating, the experiment was unable to obtain the second line of signal (lower frequency of Neon source). Using a diffraction grating with an angle of approximately 40 degrees improved signal readings. However, the additional 100 mm plano-cylindrical lens resulted in a wider signal image and increased the Neon light beam entering the 100 um slit, causing some signal loss. In conclusion, the experiment could only achieve an inconclusive image mode of the known Neon source wavelengths, while the desired outcome was sharp peaks and a spectrum covering both high and low frequencies.

## **Phase 2:**

The system underwent a significant hardware change, specifically in the spectrograph, while retaining the same underlying principles. The previous setup failed to provide accurate readings from the neon source, leading to the adoption of a new spectrograph, the HoloSpec VPH System from Kaiser Optical Systems, Inc. Unlike the previous configuration, this spectrograph did not require internal optical lens adjustments as it was optimized for experimentation. However, external hardware components were added to facilitate signal transmission to the spectrograph.

The setup included a rod-mounted Reichert 20x microscopic lens placed in front of the spectrograph's slit opening, followed by a 2" diameter 5mm biconvex lens to enhance the reception of scattered signals from the sample. A half-inch 45° prism was positioned in front of the biconvex lens to redirect laser light to the sample (Figure 5). The choice of the larger biconvex lens behind the prism aimed to improve the collection of backscattered signals. Testing the neon source with this setup successfully displayed the desired spectrums (high and low), confirming its functionality.

The HeNe 633 nm CW laser was the current light source, placed parallel to the spectrograph. A 45° mirror redirected the light beam to the prism. Neutral density filters were used for alignment, with the 633 nm optical filter removed to detect the HeNe laser signals. Alignment tests produced sharp peaks on the computer data display.

However, when attempting Raman signal detection from sulfur using the 1.0 OD neutral density filter, no signals were detected. Even after removing the filter, no Raman signals were received. The prism and biconvex lens were then removed, and the sample was positioned closer to the 633 nm optical filter, but adjustments were needed for direct alignment with the optical filter and microscopic lens.

In summary, the schematic configuration worked well for neon source calibration and HeNe laser alignment, producing two neon source spectrums and a sharp HeNe laser peak. However, detecting Raman signals from sulfur proved challenging, likely due to the setup configuration. The main issue appeared to be the prism blocking most backscattered signals from reaching the 2" biconvex lens, which was too small for efficient signal collection. Proposed solutions included using a beam splitter and an additional small biconvex lens between it and the sample to improve backscattered signal collection without component interference.

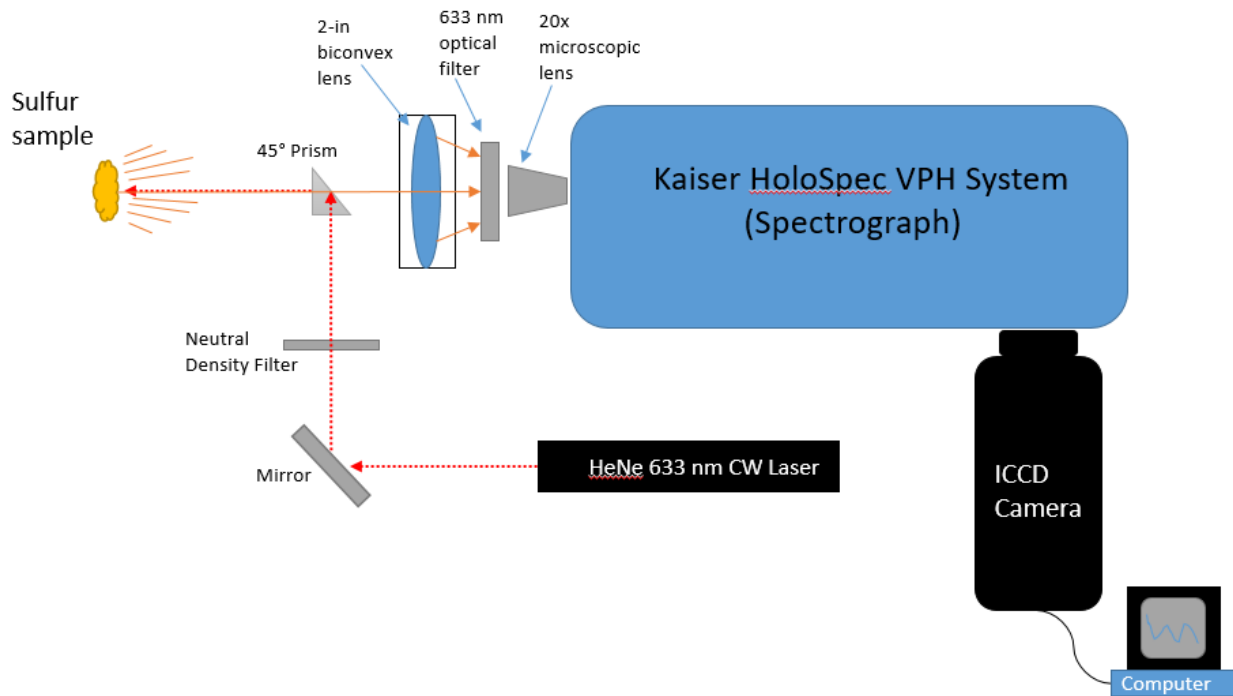


Figure 4: Block diagram for Phase 2 setup

### Phase 3:

There was another adjustment made to the system, shown in Figure 5. The orientation remained the same, while the new system featured an update to the optical system, and a 785 nm CW laser replaced the previously 632.8 nm HeNe laser as the light source. The 2-in biconvex lens was removed and replaced with a 785 nm notch filter. The 50 mm lens was placed behind the beam splitter, while the 150 mm biconvex lens was placed in front of the beam splitter. The effective focal length (EFL) of both lenses was calculated to be 6.5 cm using Equation 1, where  $f_1$  is the focal length of the first lens,  $f_2$  is the focal length of the second lens, and  $d$  is the distance between the two lenses.

$$\text{EFL} = (1/f_1) + (1/f_2) - (1/d) \quad \text{---Equation 1}$$

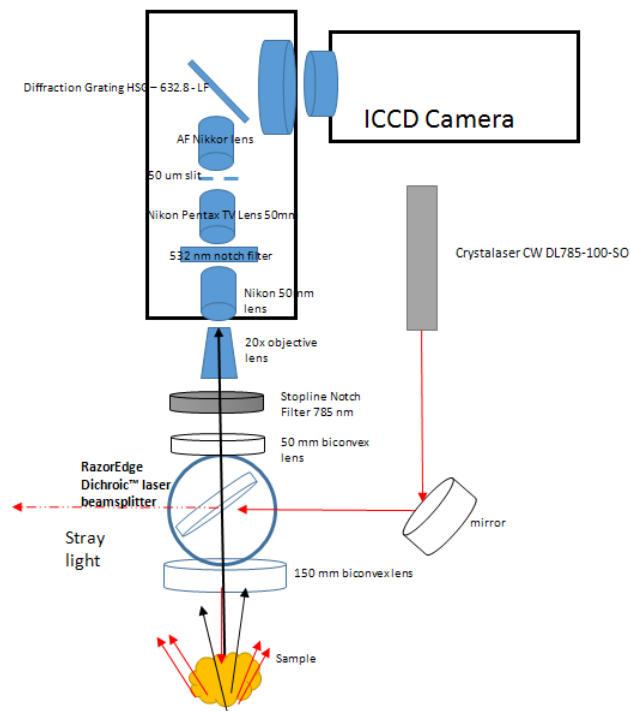


Figure 5: Top view of the block diagram of the system in Phase 3.

This updated setup output a better spectrum of the neon source, as well as detecting some strong signals, which seemed to be Anti-Stokes scattering of a solid sulfur sample. The full spectrum of the neon source can be seen in Figure 6 and it was compared to the neon calibration sheet available in the lab. Cross sections were taken from the lower and upper regions of the neon source and converted to the spectrometer mode, shown in Figure 7. Being able to detect the full spectrum of the neon source partially proved the system was working properly.

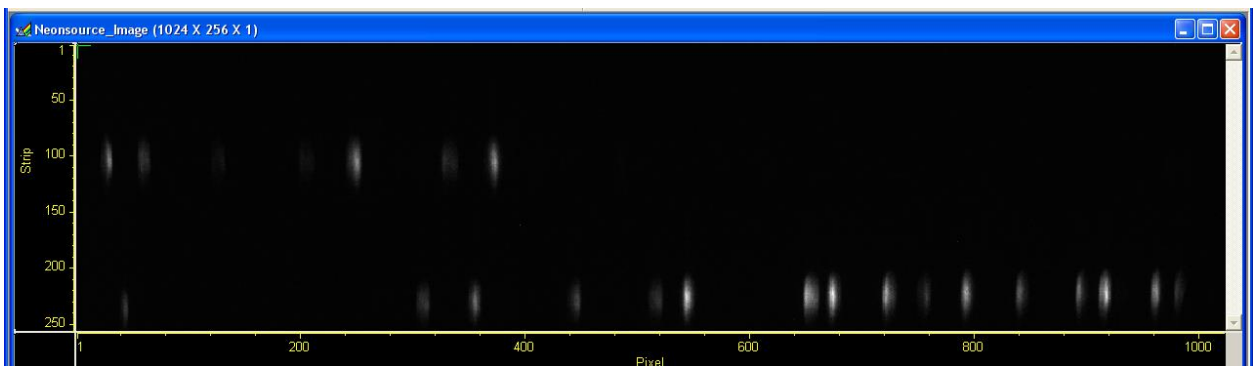


Figure 6: Image mode of the neon source, displaying both lower and upper regions.

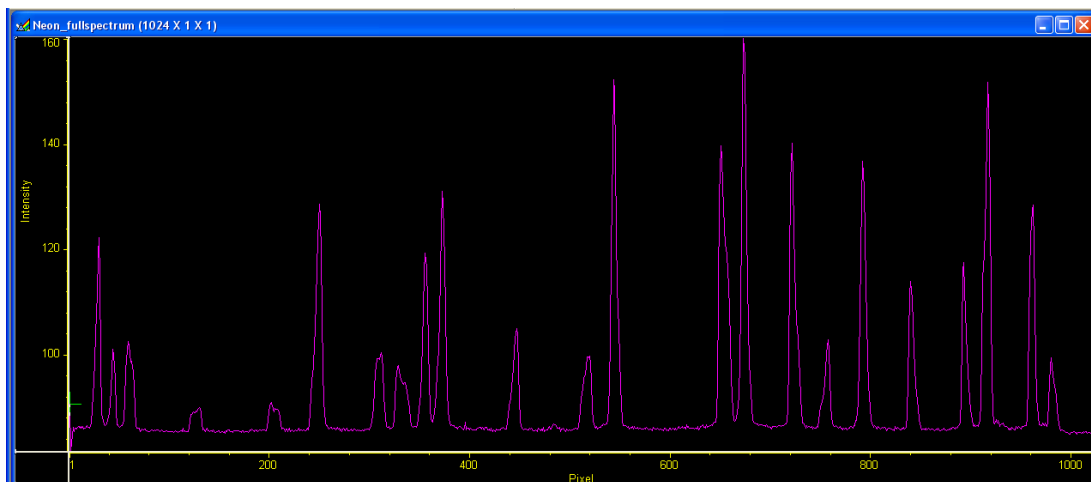


Figure 7: Peaks in lower and upper regions of the neon source.

The next Raman signal detection was done with a solid sulfur sample, also with the 785 nm CW laser light source. The left most three peaks appeared to be unique since they disappeared when the sample was blocked from the laser in Figure 8. Meanwhile, the rightmost two peaks appeared to be the 785 nm laser and leakage from background noise.

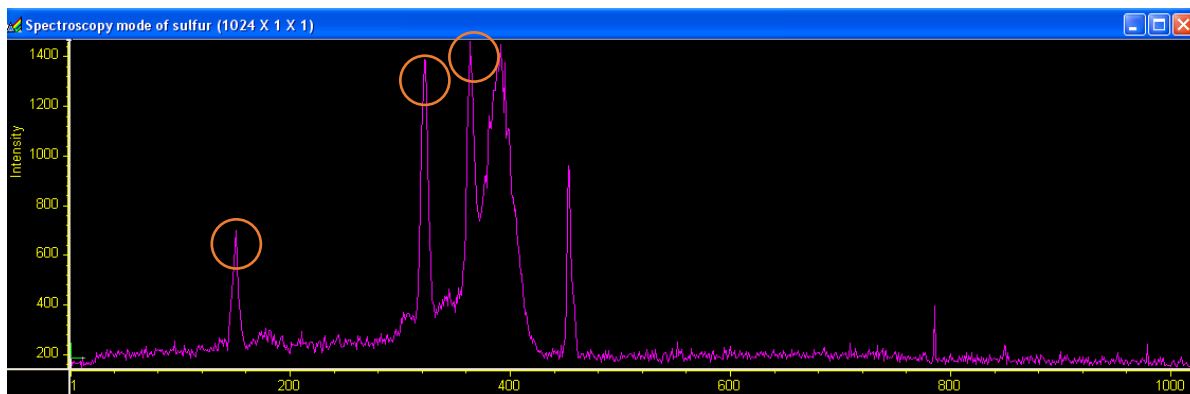


Figure 8: Peaks obtained from sulfur sample with a 785 nm CW laser, circled.

### 3. Overall Results and Analysis

To understand the relationship between pixel and the wavelength, a first-order linear relationship was used to derive an equation, using two chosen peaks of known neon wavelengths and the coordinates from the plot (wavelength, pixel) from Figure 7:

(621.72812, 184) and (638.29917, 351).

$$\begin{aligned} \text{nm/pixel} &= (\text{wavelength2} - \text{wavelength1}) / (\text{pixel2} - \text{pixel1}) && - \text{Equation 2} \\ &= ((638.29917 - 621.72812) / (351 - 184)) = 0.099 \text{ (nm/pixel)} \end{aligned}$$

Using regression analysis on the collected pixel and intensity data, the intercept is 603.55017.

The equation to better understand the pixel and wavenumber relationship is then determined in equation 2.

$$\text{Wavelength (nm)} = [0.099(\text{nm/pixel}) * \text{pixel}] + 603.55017 \quad - \text{Equation 3}$$

Based on equation 3, the predicted wavelength for the two coordinates are:

True wavelength(nm)	Pixel	Calculated wavelength(nm)	Difference
621.72812	184	621.76617	-0.03805
638.29917	351	638.29917	0

Figure 9: Pixel to wavelength conversion values.

#### Raman shift equation:

$$\Delta\nu = \frac{1e7}{\lambda_i} - \frac{1e7}{\lambda_r} \quad - \text{Equation 4}$$

$\lambda_i$  is the incident light (laser) wavelength and  $\lambda_r$  is the Raman wavelength

Naphthalene peaks were also unable to be detected by the 785 nm laser in this setup and most likely a laser with more excitation power may be needed. A 632.8nm laser was available; however, there was no 632 nm notch filter to use in the optical set up. Solid calcite sample was also not detected with the 785 nm CW laser setup; however, the laser peak intensified whenever calcite was illuminated by the incident light. Sulfur peaks were presumed to be observed, as shown in Figure 8. However, after a pixel to wavelength conversion (Equation 3) and wavelength to Raman shift (Equation 4), the peaks appeared to be Anti-stokes scattering. Unfortunately, the shift values are unusual; therefore the Raman shift plot for sulfur in Figure 10 is inconclusive.

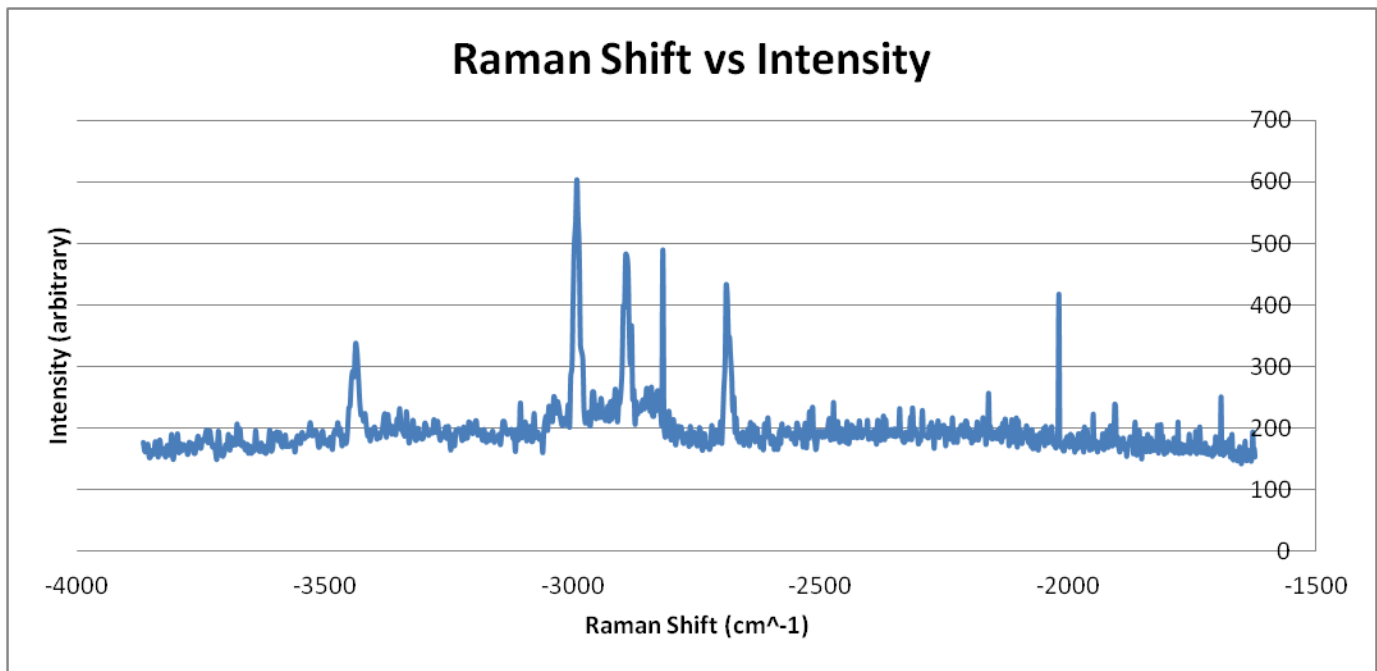


Figure 10: Calculated Raman shift for sulfur. Inconclusive.

#### 4. Summary / Conclusion

The experiment did not achieve the desired outcome, as no clear Raman signal was detected, and the obtained peaks were attributed to background radiation. Several reasons for these issues were considered. Firstly, it is necessary to thoroughly review the components' specifications to ensure correct implementation. Secondly, the optical setup requires more improvement to the alignment to achieve proper beam collimation.

Additionally, it was recognized that the optical setup, excluding the spectrometer, needed to be shielded with dark cloth to prevent deflections and background radiation. This would significantly reduce Rayleigh scattering and enhance Raman signal detection. Another option was to explore a simpler optical setup that could eliminate using the dichroic beam splitter, which might have been used incorrectly.

A baseline correction will be necessary to find hidden Raman signals [11]. Baseline correction can be accomplished by polynomial fitting, subtraction of a reference spectrum or perhaps create or obtain specialized software tools that can automatically adjust the baseline to improve the clarity and accuracy of peak identification and quantification. These are other methods that may help highlight the true Raman signals and assist in the interpretation of the spectral data. As such, the knife-edge method for beam spot sizing could be utilized to characterize the profile of the beam.

Despite the advantages of Raman spectroscopy, limitations such as fluorescence interference, background radiation, and the need for high laser power were acknowledged. To enhance the experiments, beam shaping, precise optical alignment, and a better understanding of component

usage, especially for collimating the beam and reassessing the dichroic beam splitter's specifications, were identified as necessary improvements.

## 5. References

- [1] “Raman Microscope Overview – US,” *www.thermofisher.com*.  
<https://www.thermofisher.com/us/en/home/industrial/spectroscopy-elemental-isotope-analysis/molecular-spectroscopy/raman-microscopy.html>
- [2] G. S. Christopher, Nurul M. Abedin, S. K. Shiv, M. K. Anupam, I. Syed, S. P. Stephen, H. Elsayed-Ali, “Remote Raman sensor system for testing of rocks and minerals,” *Sensors, and Command, Control, Communications, and Intelligence (C3I) Technologies for Homeland Security and Homeland Defense VI*, vol. 6538 65381I-1, 2007.
- [3] G. S. Christopher, Nurul M. Abedin, S. K. Shiv, M. K. Anupam, I. Syed, S. P. Stephen, H. Elsayed-Ali, “Remote Raman sensor system for testing of rocks and minerals,” *Sensors, and Command, Control, Communications, and Intelligence (C3I) Technologies for Homeland Security and Homeland Defense VI*, vol. 6538 65381I-1, 2007.
- [4] G. S. Christopher, Nurul M. Abedin, I. Syed, S. K. Shiv, M. K. Anupam and S. P. Stephen, H. Elsayed-Ali, “Design and build a compact Raman sensor for identification of chemical composition,” *Sensors, and Command, Control, Communications, and Intelligence (C3I) Technologies for Homeland Security*, vol. 6943 69430I-1, 2008.
- [5] Walter, E. C. Le, P.T. Northcote, and P. Etchegoin. “High performance Raman spectroscopy with simple optical components,” *American Journal of Physics*, vol.78, no.7, pp.671-677, Jun. 2010, doi: <https://doi.org/10.1119/1.3427413>
- [6] “What are the basic principles of Raman Spectroscopy?,” *Oxford Instruments*.  
<https://andor.oxinst.com/learning/view/article/raman-spectroscopy>
- [9] Bruker, “Guide to Raman Spectroscopy,” *www.bruker.com*.  
<https://www.bruker.com/en/products-and-solutions/infrared-and-raman/raman-spectrometers/what-is-raman-spectroscopy.html>
- [10] P. Whiteaker, “Calibration and Validation of Raman Instruments,” *Elodiz*.  
<https://www.elodiz.com/calibration-and-validation-of-raman-instruments/>
- [11] “Technology Highlight The Challenge Our Solution Improved Performance Baseline Correction Methods for Raman Spectroscopy VTIP 20-065: ‘ISREA: An Efficient Peak-preserving Baseline Correction Algorithm for Raman Spectra.’” Accessed: Dec. 07, 2023. [Online]. Available: [https://www.vt.edu/content/dam/link\\_vt\\_edu/vtip/toa-docs/toa-20-065.pdf](https://www.vt.edu/content/dam/link_vt_edu/vtip/toa-docs/toa-20-065.pdf).